Supporting Information

Compositional and interfacial engineering for improved light stability of flexible wide-bandgap perovskite solar cells

Anna Wąsiak-Maciejak, Łukasz Przypis, Wiktor Żuraw, Kinga Rycek, Patrycja Janicka, Mateusz Ścigaj, Konrad Dyk, Adrianna Piejko, Huagui Lai, Damian Pucicki, Vasyl Kinzhybalo, Fan Fu, and Konrad Wojciechowski*

Materials synthesis

Commercially available chemicals were used without further purification. Oxindole (98.0%, AmBeed), phosphoryl chloride (POCl3, 99.0%, Sigma-Aldrich Co), triethylphosphite (98.0%, Sigma-Aldrich Co) potassium tert-buthoxide (99.99%, Sigma Aldrich), 1,4-dibromobutane (99.0%, Sigma-Aldrich Co), bromotrimethylsilane (98.0%, Acros), potassium hydroxide (99.0%, Sigma-Aldrich Co) Dimethylformamide (DMF anhydrous, Sigma-Aldrich Co), dichloromethane, cyclohexane, ethyl acetate, toluene, methanol and acetone were purchased from Sigma-Aldrich Co.

Synthesis

All reactions were carried out under an argon atmosphere in oven-dried glassware with magnetic stirring. Analytical thin-layer chromatography (TLC) was performed on silica gel 60 TLC plates. The spots were visualized with a UV light or by staining with $KMnO_4$ or anisaldehyde solution. Flash column chromatography was performed using silica gel 60 (particle size 0.040−0.063 mm), typically using a cyclohexane/ethyl acetate eluent system. Reported yields are based upon isolation following purification by silica gel column chromatography; isolated materials were judged to be homogeneous based on TLC and NMR.

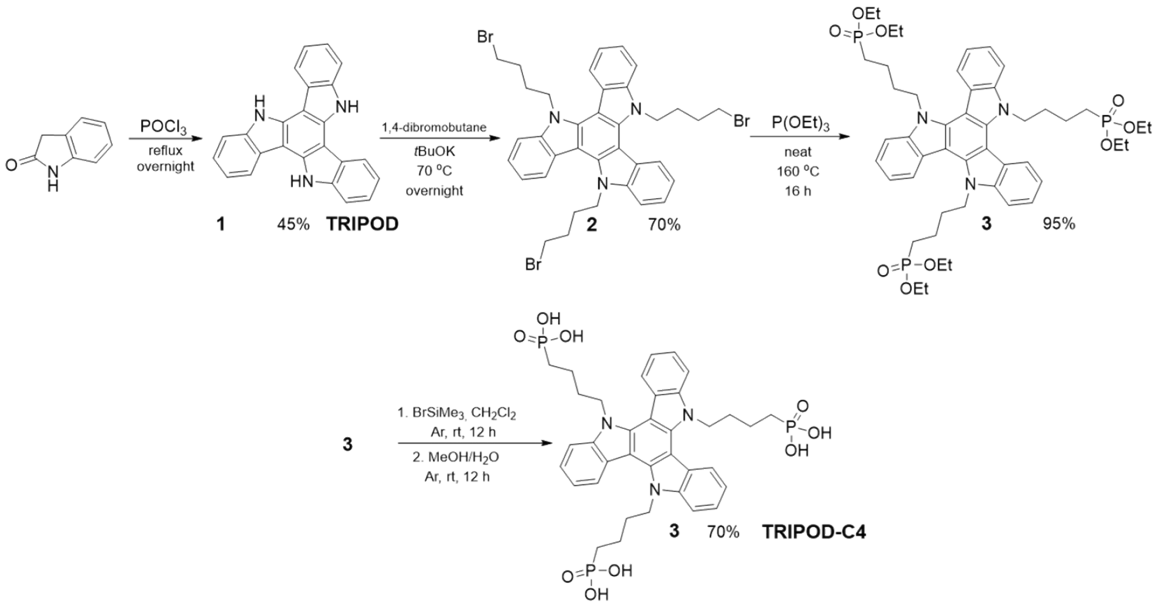

Figure S1. Reaction pathway for the synthesis of the *TRIPOD-C4* compound.

Synthesis of 15-dihydro-5H-diindolo[3,2-a:3',2'-c]carbazole (1, TRIPOD):

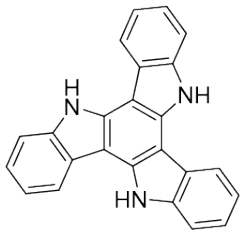

Under an argon atmosphere using a Schlenk line, oxindole (16.1 g, 121.21 mmol) was dissolved in $POCl_3$ (75 mL) and the resulting solution was stirred and refluxed overnight. After cooling to room temperature, the dark brown mixture was cautiously poured into ice water and carefully neutralized with NaOH. The resulting brown precipitate was filtered off to give the crude product. The crude product was purified by silica gel column chromatography using a dichloromethane/ ethyl acetate (1:1) mixture as the eluent. Then was evaporated under reduced pressure, and the residue was fractional recrystallized from toluene and acetone to yield compound **1** as a beige solid (9.4 g, 17.89 mmol, 44% yield). **^{1}H NMR** (400 MHz, DMSO-d_6): δ 7.27–7.37 (m, 6H), 7.68–7.70 (m, 3H), 8.64 (d, J = 8.0 Hz, 3H), 11.84 (s, 3H) **^{13}C NMR** (101 MHz, DMSO-d_6): δ 103.2, 111.8, 120.5, 121.9, 123.0, 123.5, 138.5, 141.1.

Synthesis of 5,10,15-tris(4-bromobutyl)-10,15-dihydro-5H-diindolo[3,2-a:3',2' c]carbazole (2):

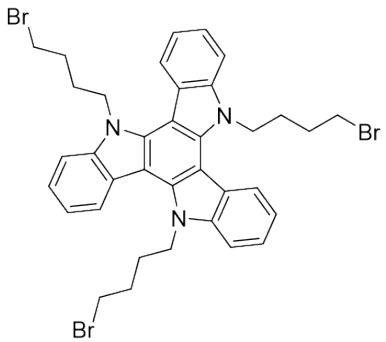

To a solution of compound **1** (1.00 g, 2.90 mmol) in anhydrous DMF (30 mL), *t*BuOK (418 mg, 17.40 mmol) was added at room temperature and the mixture was stirred for 10 minutes. Next, 1,4-dibromobutane (5.4 mL, 45.00 mmol) was added via syringe, and the reaction mixture was stirred for 2 hours at 70 °C. The reaction mixture was then poured into water, washed with brine, and extracted with dichloromethane. The organic phase was dried over Na_2SO_4, filtered, and concentrated under reduced pressure to yield the crude product. The crude product was purified by silica gel column chromatography using a cyclohexane/ethyl acetate mixture (6:1 to 1:1) as the eluent, yielding 1.52 g of compound **2** (2.03 mmol, 70% yield) as a beige solid. **^{1}H NMR** (400 MHz, $CDCl_3$): δ 1.62–1.73 (m, 6H), 2.06–2.11 (m, 6H), 3.24 (t, J = 7.0 Hz, 6H), 4.94 (t, J = 7.2 Hz, 6H), 7.32–7.40 (m, 3H), 7.46–7.50 (m, 3H), 7.65 (d, J = 8.0

Hz,3H), 8.22–8.24 (d, J = 8.0 Hz, 3H). **^{13}C NMR** (101 MHz, $CDCl_3$): δ 28.5, 30.1, 33.0, 46.1, 104.0, 110.7, 120.2, 121.5, 123.2, 123.5, 138.1, 141.0.

Synthesis of 5,10,15-tris(4-bromobutyl)-10,15-dihydro-5H-diindolo[3,2-a:3',2'-c]carbazole (3):

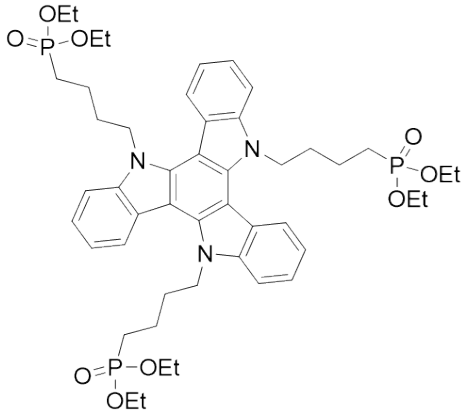

Compound **2** (525 mg, 0.70 mmol) was dissolved in triethylphosphite (5 mL) under an inert atmosphere, and the reaction mixture was stirred at 160 °C overnight. After cooling to room temperature, the solvent was removed under reduced pressure to yield the crude product. The crude product was purified by vacuum distillation to obtain 571 mg of compound **3** (0.62 mmol, 95%) as a pale-yellow oil. **^{1}H NMR** (400 MHz, $CDCl_3$): δ 1.18 (t, J = 7.2 Hz, 18H), 1.48–1.70 (m, 12H), 1.96–2.07 (m, 6H), 3.91–4.00 (m, 12H), 4.93 (t, J = 7.6 Hz, 6H), 7.32–7.37 (m, 3H), 7.40–7.47 (m, 3H), 7.61–7.64 (d, J = 8.1 Hz, 3H), 8.21–8.24 (d, J = 8.1 Hz, 3H). **^{13}C NMR** (101 MHz, $CDCl_3$): δ 16.4, 20.0, 25.2, 30.5, 46.0, 61.7, 103.9, 110.8, 120.6, 121.3, 123.0, 123.6, 138.8, 141.0.

Synthesis of ((5H-diindolo[3,2-a:3',2'-c]carbazole-5,10,15-triyl)tris(butane-4,1-diyl))tris(phosphonic acid) (4, *TRIPOD-C4*):

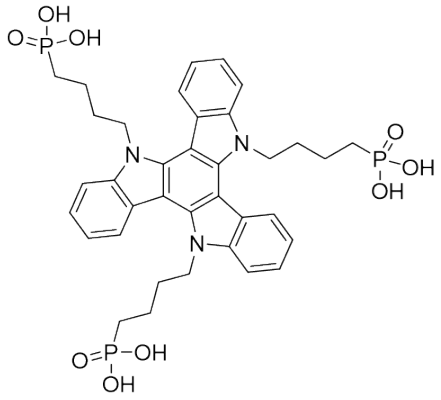

Under an argon atmosphere (Schlenk line), compound **3** (200 mg, 0.23 mmol) was dissolved in dry dichloromethane (6 mL). Then, bromotrimethylsilane (500 µl, 3.85 mmol) was added dropwise. The reaction mixture was stirred at room temperature for 14 hours. Next the

solvent was removed under reduced pressure, the solid residue was suspended in mixture of methanol and water (3:1, v/v). The precipitate was filtered and washed with dichloromethane to give 125 mg of 4 (0.18 mmol, 77% yield) as a bluish powder. **^{1}H NMR (400 MHz, DMSO-d_6):** δ 1.18–1.50 (m, 12H), 1.80–1.95 (m, 6H), 4.96 (t, J = 6.7 Hz, 6H), 7.28–7.39 (m, 3H), 7.40–7.52 (m, 3H), 7.84 (d, J = 6.8 Hz, 3H), 8.26 (d, J = 6.7 Hz, 3H). **^{13}C NMR (101 MHz, DMSO-d_6):** δ 22.4, 27.7, 30.2, 46.0, 102.6, 111.0, 120.0, 121.3, 122.5, 123.0, 138.0, 140.6. **^{31}P NMR (162 MHz, DMSO-d_6):** δ 27.09. **HRMS (ESI) m/z:** [M+H] Calcd for $C_{36}H_{43}N_3O_9P_3$ 754.2212; Found: 754.2211.

Characterization methods

Nuclear magnetic resonance (NMR)

NMR spectra were measured at room temperature on a Bruker 400 MHz spectrometer. NMR spectra were calibrated to the solvent residual signals of $CDCl_3$ (δ = 7.26 ppm in ^{1}H NMR, δ = 77.16 ppm in ^{13}C NMR) or DMSO-d_6 (δ = 2.50 ppm in ^{1}H NMR, δ = 39.50 ppm in ^{13}C NMR). ^{1}H NMR spectra were recorded at 400 MHz. Data are reported as follows: chemical shift, multiplicity (s: singlet, d: doublet, t: triplet, m: multiplet), coupling constant (J in Hz), and integration. ^{13}C NMR spectra were recorded at 101 MHz using broadband proton decoupling, and chemicals shifts are reported in ppm using residual solvent peaks as reference. ^{31}P NMR spectra were recorded at 162 MHz.

High-resolution mass spectra (HRMS)

HRMS spectra were recorded on an MS (ESI) spectra LCMS-IT TOF Shimadzu or SYNAPT G2-S HDMS (Waters).

Fourier transform infrared spectroscopy (FTIR) measurements

FTIR measurements of PET-IZO/NiO_X and PET-IZO/NiO_X/SAM were performed with a Bruker Vertex 80v spectrometer.

Ultraviolet photoelectron spectroscopy (UPS)

UPS measurements were performed with a non-monochromatic excitation source of 21.2 eV. Photoelectrons were collected by a hemispherical electron energy working in a constant analyser energy mode (CAE) with a step size of 0.05 eV or 0.1 eV and a pass energy of 20 eV in case of XPS measurements. A step size of 0.025 eV and a pass energy of 2 eV were applied for UPS experiments. All binding energies (BEs) were referred to the Fermi level (E_F), the position of which was determined using an Ar-ion cleaned reference Ag sample.

Current density-voltage (J-V) measurements

J-V measurements were conducted under simulated AM1.5G irradiation (100 mA/cm^2) using an AAA-rated solar simulator Sun 2000 from Abet Technologies, calibrated with an RR-208-KG5 silicon reference cell from Abet Technologies. J-V measurements were performed in two scan directions: from forward bias to short-circuit (reverse) and from short-circuit to forward

bias (forward), with a scanning rate of 0.5 V/s. The stabilized power output (SPO) was measured at the maximum power point voltage from the best J-V scan for 28 seconds. The solar cells were masked to 0.64 cm².

Steady-state photoluminescence measurement (ss-PL)

Steady-state photoluminescence measurements were conducted using a hyperspectral imaging microscope from Photon Etc., equipped with a 532 nm wavelength green laser as the excitation source. Photoluminescence mapping and analysis were performed using the hyperspectral imager IMA-VISTM from Photon Etc.

Time-resolved photoluminescence measurement (TRPL)

TRPL measurements were conducted using an FS5 spectrofluorometer (Edinburgh Instrument) equipped with a time-correlated single photon counting (TCSPC) unit. The PET/perovskite and PET-IZO/NiO_X/SAM/perovskite films were excited from the perovskite side with a 405 nm laser diode at an excitation intensity of 15 mW/cm².

Ultraviolet-visible (UV-VIS) spectroscopy

The UV-Vis absorption spectra were measured with the Edinburgh Instruments Spectrofluorometer FS5, using an Xe lamp light source.

External Quantum Efficiency (EQE)

The EQE spectra were measured using Bentham PVE300 system and the control software BenWin+. For tandem solar cells, the bias illumination from LEDs with emission peak of 850 and 450 nm were used to measure the front and back subcells, respectively. No bias voltage was applied during the EQE measurement.

Scanning electron microscopy (SEM) and focused ion beam scanning electron microscopy (FIB-SEM)

SEM images were acquired using the Phenom Pro-X microscope. FIB-SEM cross-section images were taken with the SEM/Ga-FIB Microscope FEI Helios NanoLab™ 600i.

X-ray diffraction measurement (XRD)

X-ray diffraction (XRD) diffractograms of perovskite thin films of different compositions were obtained using the Rigaku MiniFlex diffractometer with the CuKα (λ = 1.541 Å) radiation with Ni filter and generator parameters V = 40kV, I = 15mA at room temperature. Scans were performed in the range 5-50° with step size 0.01°.

Iodine release test

The experimental setup was described in detail in our previous work.[1] The approximated equivalent of released I_2 gas was calculated assuming the reaction (1).

$$2\,Ag + I_2 \rightarrow 2AgI \quad (1)$$

Time-of-Flight Secondary Ion Mass Spectrometry (TOF-SIMS)

ToF-SIMS measurements were performed with a time-of-flight secondary ion mass spectrometer (ToF-SIMS V system, ION-TOF). The primary beam was 25 keV Bi^{3+} with a total current of 0.46 pA and a raster size of 50 μm× 50 μm. Cs^{+} ions were used with 1000 eV ion energy, 60 nA pulse current on a 300 × 300 μm^2 raster size to bombard and etch the film.

Kelvin Probe Force Microscopy (KPFM)

KPFM measurements were performed with a NanoWorld ARROW-EFM probe with a force constant of ~2.8 N/m and a resonant frequency of ~75 kHz, using the AM-KPFM method in two-pass mode. In the first pass, the topography of the sample was measured, and in the second pass, an AC voltage was applied to excite the probe at the resonant frequency (lift-mode). At the same time, the DC voltage was adjusted to cancel the oscillations of the cantilever to determine the contact potential difference between the probe and the sample.

The work function of the material (φ_{sample}) was determined from the CPD results. KPFM measurements were carried out in two steps: first, calibration was performed with a material with a known work function, and then the actual material was measured. Freshly cleaved HOPG (highly oriented pyrolytic graphite) was used as the calibration sample, whose φ =4.6 eV.

Based on the CPD and φ_{tip}, the work function of the sample was calculated using equation (1).

$$\varphi_{sample} = \varphi_{tip} - e \cdot U_{CPD} \quad (1)$$

where: e is the elementary charge, while U_{CPD} is the measured contact potential difference.

Bending test

The repeated bending cycle measurements were conducted using a custom-designed one-dimensional mobile platform powered by a stepper motor.

Table S1. Full width at half maximum (FWHM) and intensity of reflexes for different perovskite compositions on PET, extracted from X-ray diffractograms.

Perovskite composition	14.2 [°]		28.9 [°]	
	Intensity [a. u.]	FWHM	Intensity [a. u.]	FWHM
Pristine	2.19	0.29	0.25	0.21
Pb-SCN	4.50	0.19	0.62	0.17
4F+Pb-SCN	53.29	0.12	7.99	0.15

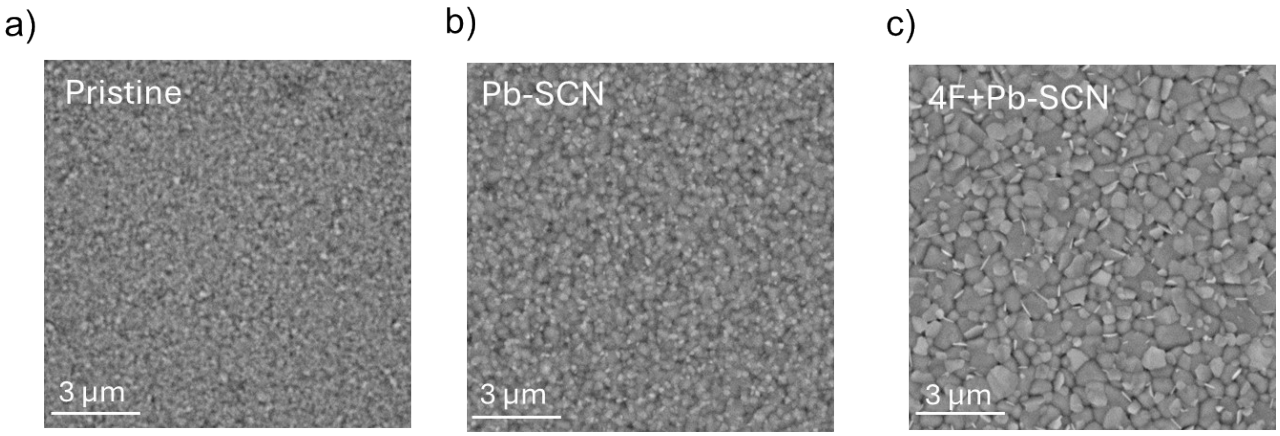

Figure S2. a-c) Top-view SEM images of perovskite thin films of different compositions (*Pristine, Pb-SCN, 4F+Pb-SCN*).

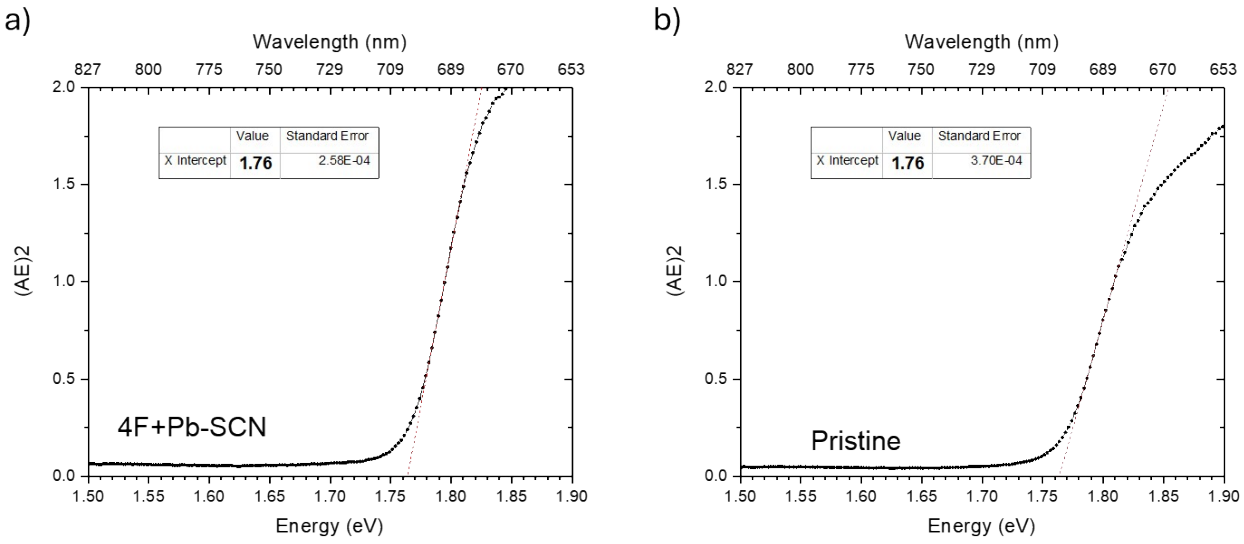

Figure S3. Tauc plots of a) *4F+Pb-SCN* and b) *Pristine* WBG perovskite composition on PET-IZO/NiO_X/*Me-4PACz*.

Table S2. Exponential function fitting parameters for the photoluminescence decay curves, measured for different WBG perovskite samples. Excitation from the perovskite side with the 405 nm laser diode, fluence of 15 nJ/cm².

Bi-exponential function fitting					
Layer stack	**A_1**	**τ_1 [ns]**	**A_2**	**τ_2 [ns]**	**R^2**
PET/*4F+Pb-SCN*	0.06	89	0.86	488	0.993
PET/*Pb-SCN*	0.30	6	0.67	137	0.998
PET/*Pristine*	9.21	4	0.09	181	0.984
Mono-exponential function fitting					
Layer stack	**A_1**	**τ_1 [ns]**	**R^2**		
PET/*4F+Pb-SCN*	0.94	423	0.993		

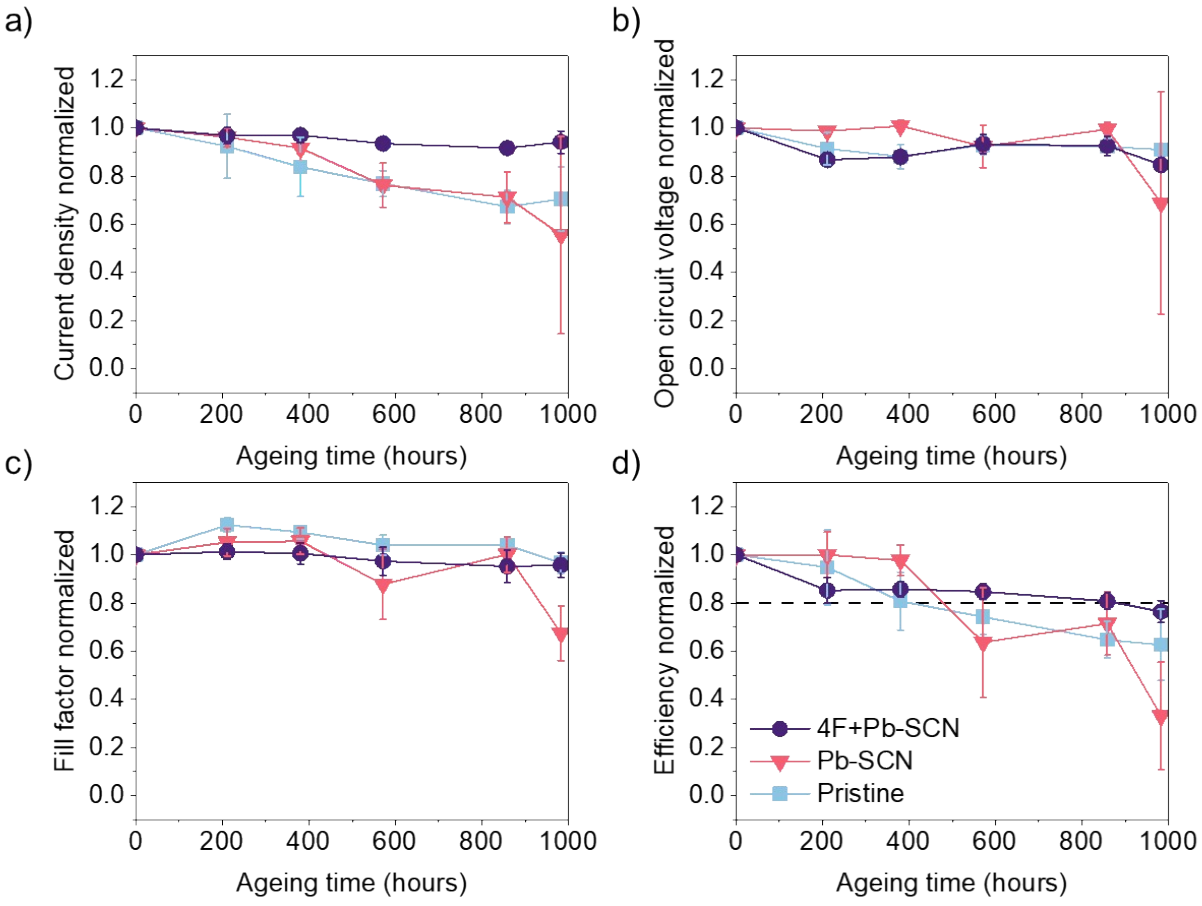

Figure S4. a-d) Evolution of normalized PV parameters of flexible WBG devices with *4F+Pb-SCN, Pb-SCN*, and *Pristine* perovskite upon light-soaking in open circuit condition at 40°C, in an inert atmosphere. Average parameters and standard deviations were derived from measurements of 2 devices.

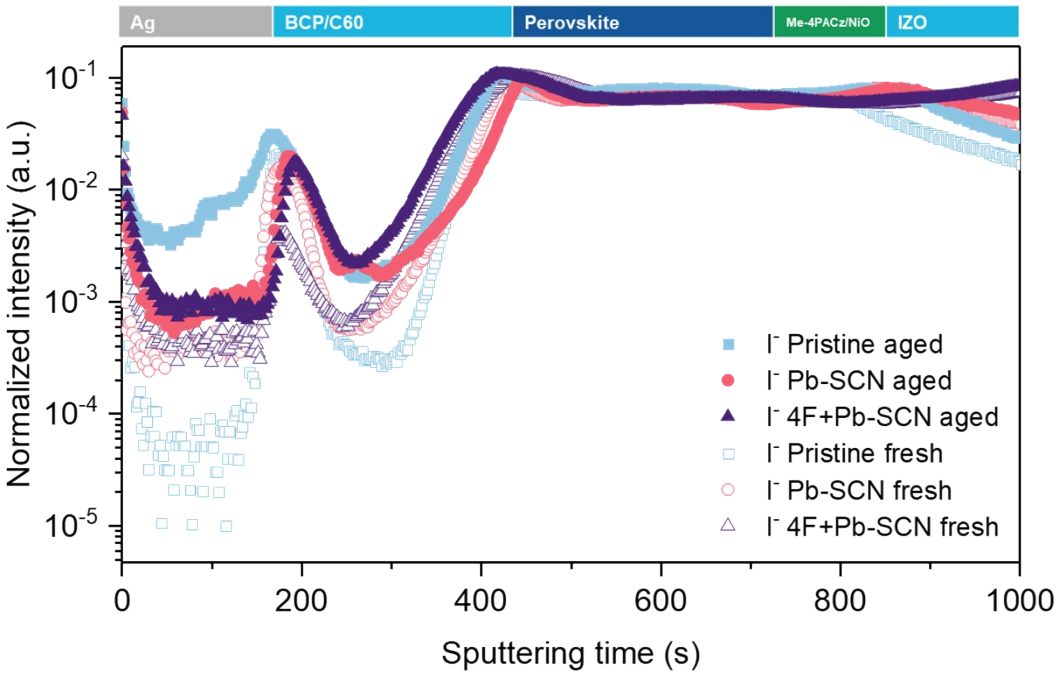

Figure S5. TOF-SIMS analysis of flexible WBG devices with *Pristine, Pb-SCN,* and *4F+Pb-SCN* perovskite composition before and after 1000 hours of light-soaking in OC conditions at 40°C, in an inert atmosphere.

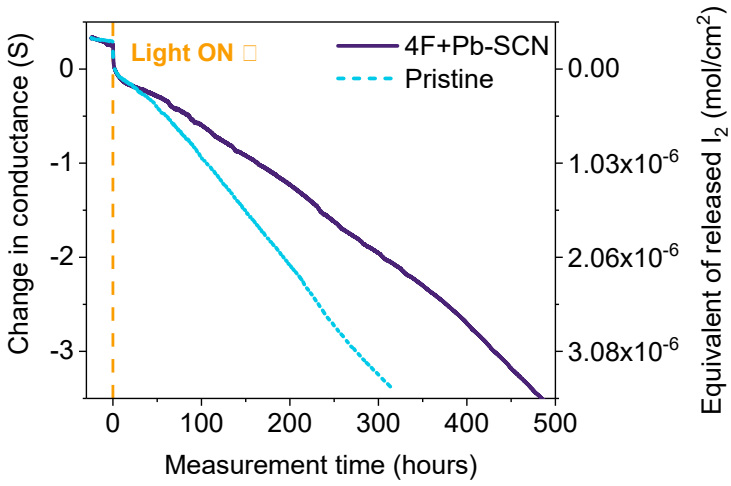

Figure S6. Time evolution of change in silver conductance and the equivalent of molecular iodine vapour released upon the light-soaking test for samples with *Pristine* and *4F+Pb-SCN* perovskite composition (average of 4 samples).

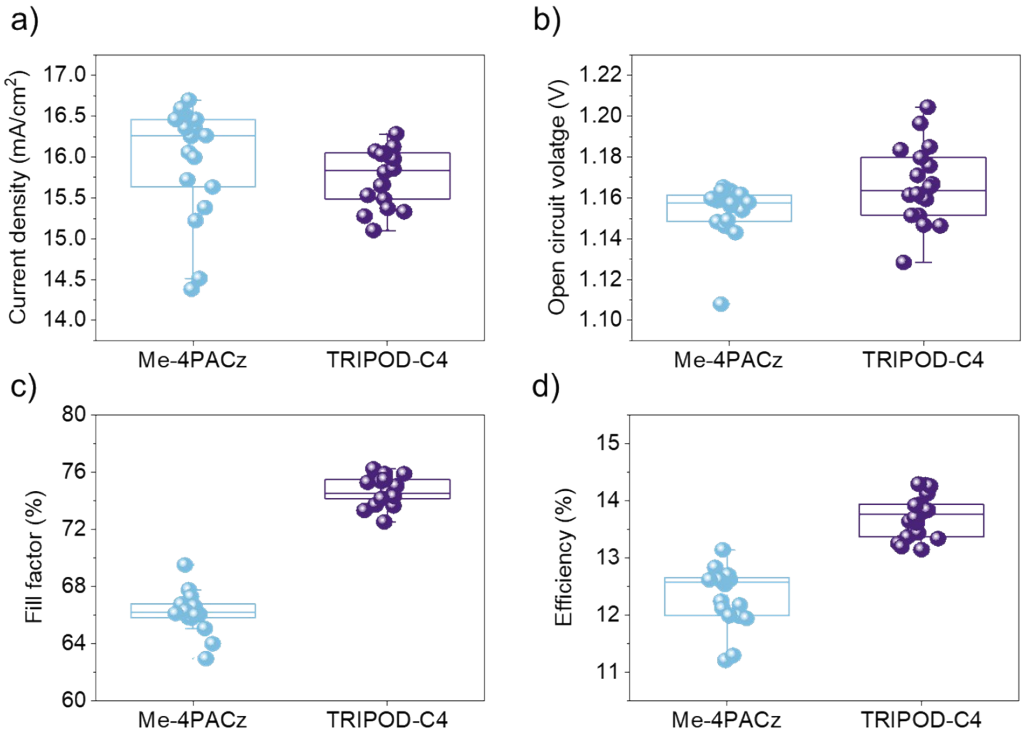

Figure S7. a-d) Statistics of photovoltaic parameters extracted from the J-V measurements of the flexible WBG devices employing *Me4PACz* and *TRIPOD-C4* as a SAM (average of 15 devices).

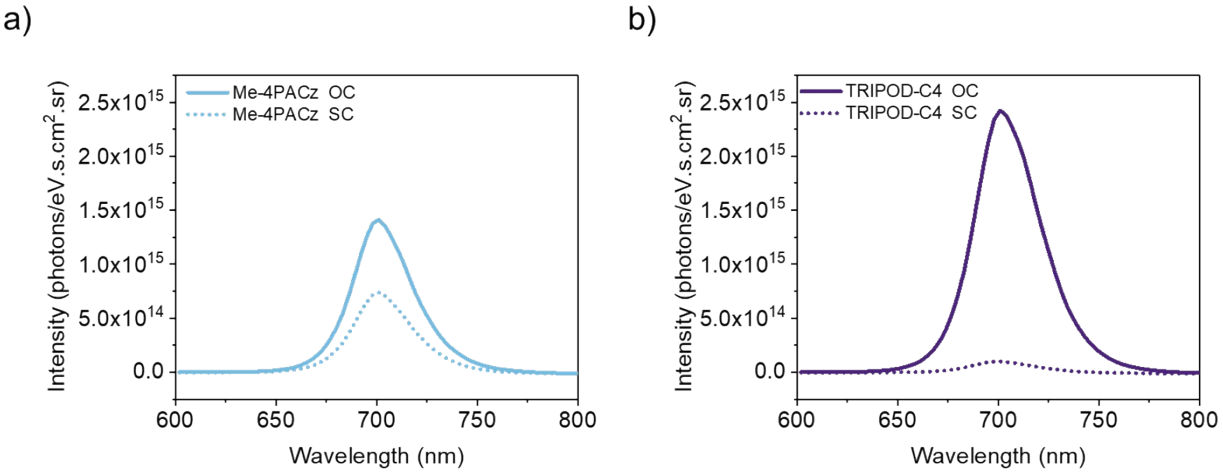

Figure S8. Absolute PL spectrum measured in open circuit ($PL_{abs,OC}$) and short-circuit ($PL_{abs,SC}$) conditions for WBG devices with: a) *Me4PACz* and b) *TRIPOD-C4* as SAM.

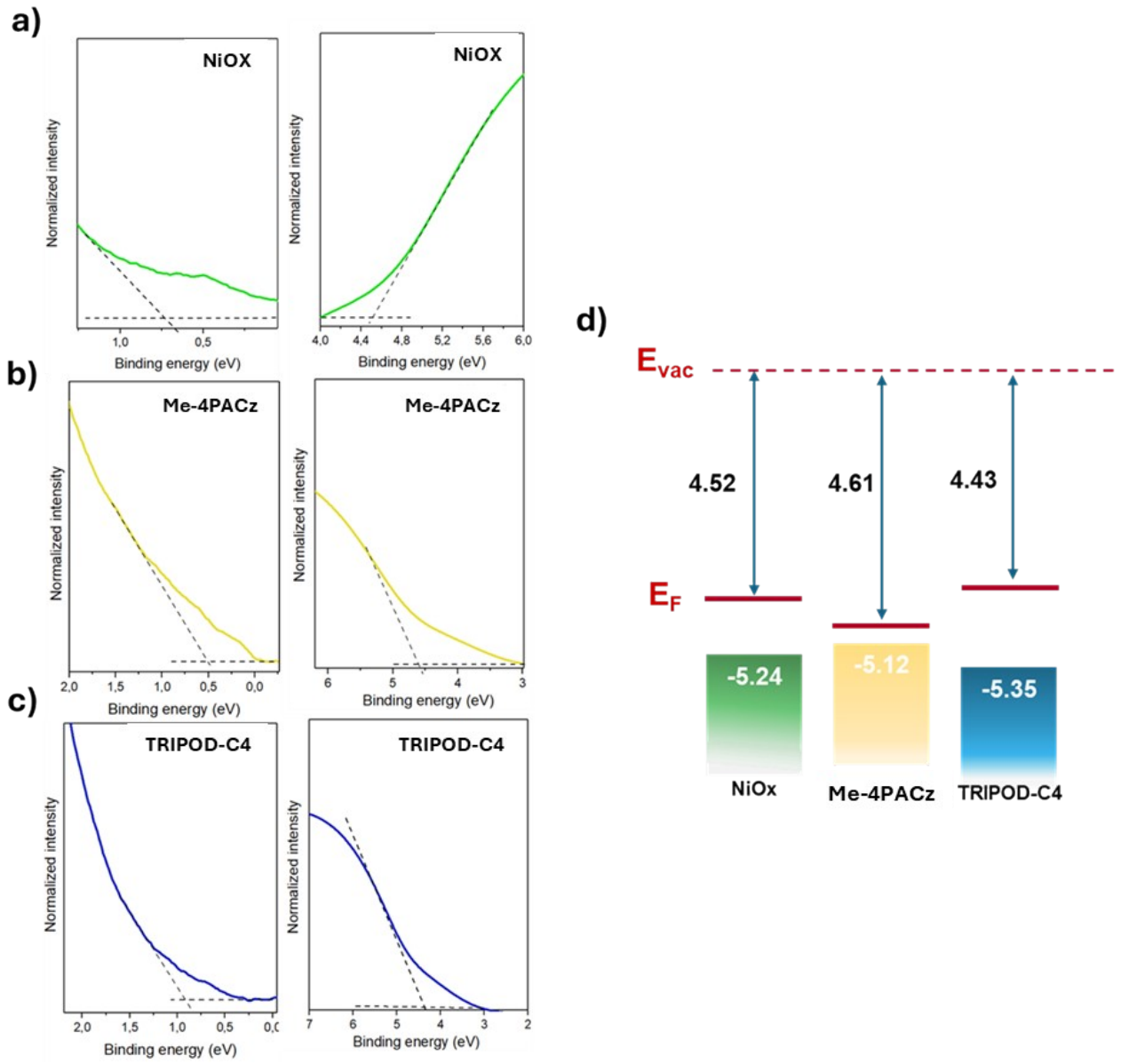

Figure S9. a-c) UPS of *NiO_X, Me4PACz, TRIPOD-C4*; d) graphical representation of Fermi level (E_f) and vacuum level (E_{vac}) of *NiO_X, Me4PACz, TRIPOD-C4.*

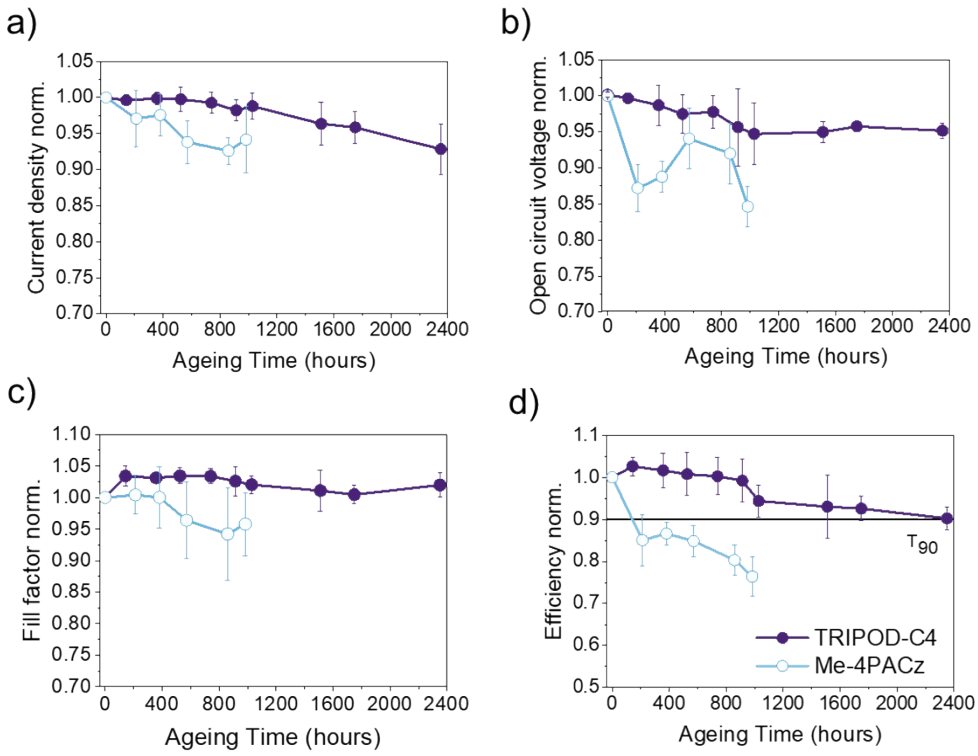

Figure S10. a-d) Evolution of normalized PV parameters of flexible WBG devices with *Me-4PACz* and *TRIPOD-C4* as a SAM upon light-soaking in open circuit condition at 40°C, in an inert atmosphere. Average parameters and standard deviations were derived from measurements of 4 devices.

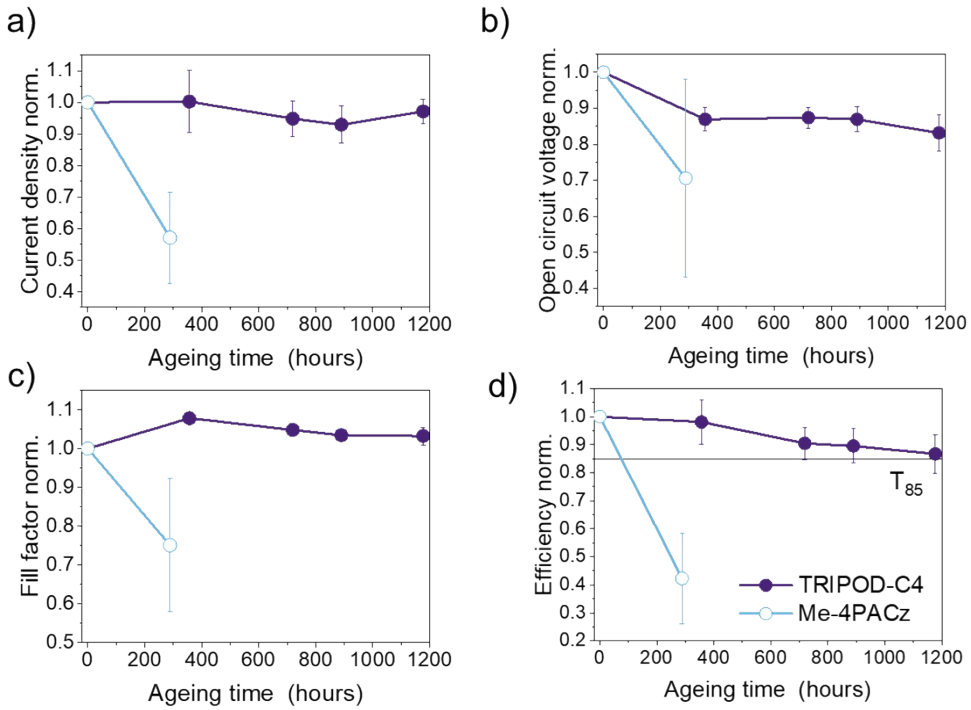

Figure S11. a-d) Evolution of normalized PV parameters of flexible WBG devices with *Me-4PACz* and *TRIPOD-C4* as a SAM upon light-soaking in open circuit condition at 65°C, in an inert atmosphere. Average parameters and standard deviations were derived from measurements of 4 devices.

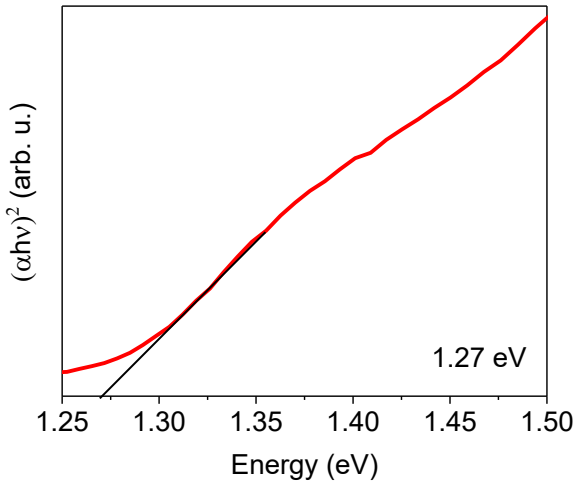

Figure S12. Tauc plot of NBG perovskite.

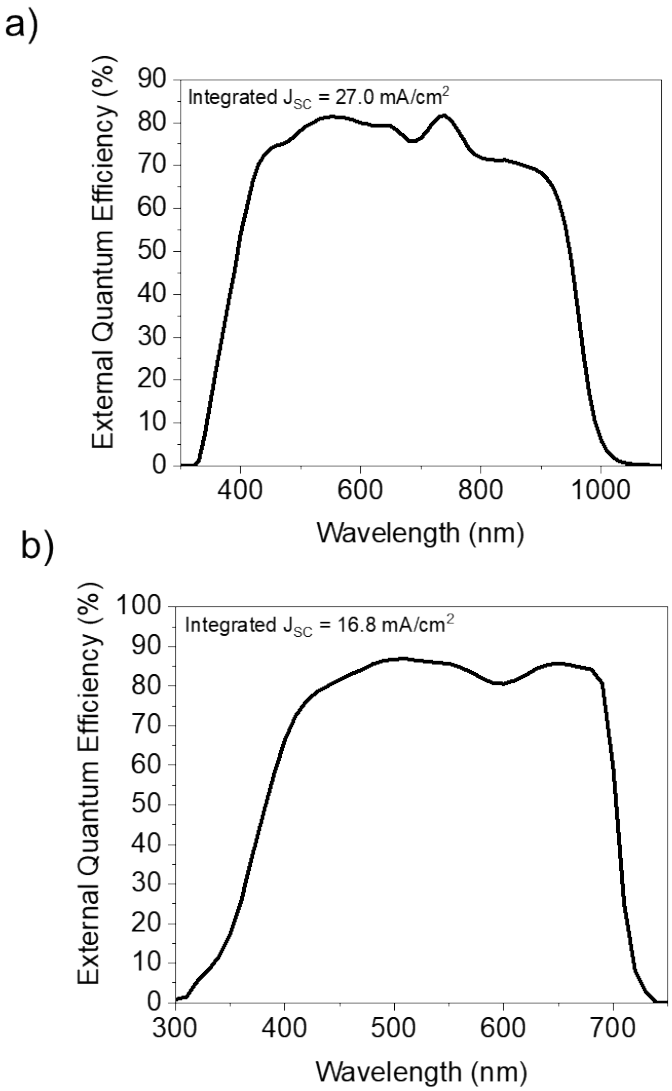

Figure S13. The external quantum efficiency of champion single-junction devices: a) NBG and b) WBG.

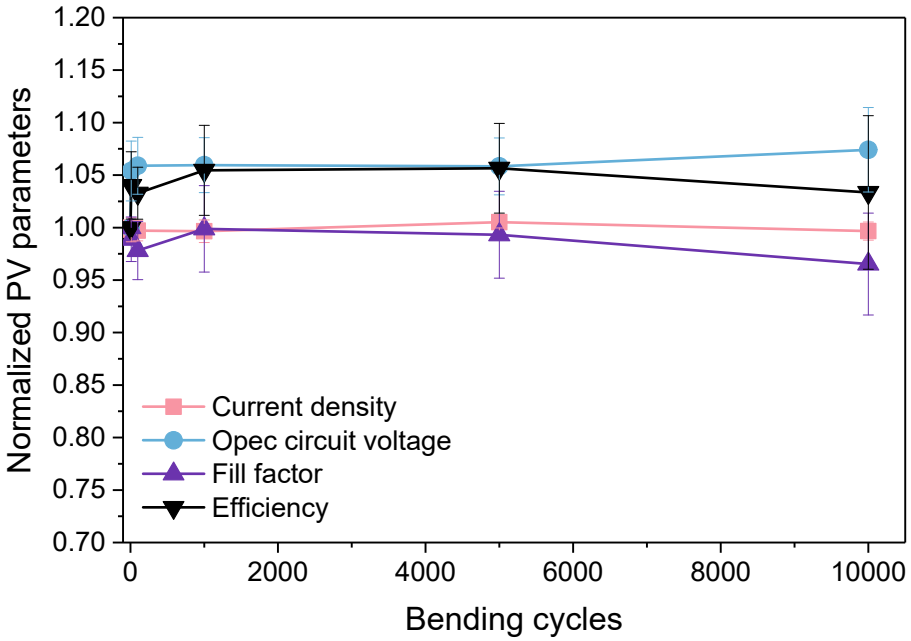

Figure S14. Evolution of normalized PV parameters of unencapsulated 1 cm^2 all-perovskite tandem solar cells, utilizing *TRIPOD-C4* as a SAM and *4F+Pb-SCN* perovskite composition subjected to the bending test with a radius of 15 mm in ambient conditions. Average parameters and standard deviations were derived from measurements of 3 devices.

References

(1) S. Dasgupta, W. Żuraw, T. Ahmad, L. A. Castriotta, E. Radicchi, W. Mróz, M. Ścigaj, Ł. Pawlaczyk, M. Tamulewicz-Szwajkowska, M. Trzciński, J. Serafińczuk, E. Mosconi, A. Di Carlo, F. De Angelis, A. Dudkowiak, K. Wojciechowski, *ACS Appl Energy Mater* **2022**, *5*, 15114.